IEEJ Journal of Industry Applications
Vol.8 No.4 pp.669–676 DOI: 10.1541/ieejjia.8.669

Paper

High Power/Current Inductor Loss Measurement with Improved Shunt Resistor Construction

Pin-Yu Huang[*a)] Member, Toshihisa Shimizu[**] Fellow

(Manuscript received Aug. 1, 2018, revised March 19, 2019)

The increasing requirement for high-power-density converters has resulted in the need for accurate analysis of the power loss of inductive components. Some inductors are operated at high frequency and current. However, the maximum AC ripple current measurement range of B–H analyzer, which is a high precision measurement device, is ±6 A. In this paper, a low-cost measurement method using the shunt resistor as a high current sensor is proposed. To abbreviate the measurement deviation caused by the parasitic inductance of shunt resistor, the Runge-Kutta calculation method is applied to determine the inductor current. Furthermore, a shunt resistor connection configuration is proposed to reduce the influence of parasitic inductance. To demonstrate the feasibility of this method, an inductor is measured under 160 A (RMS) current, 10 kHz switching frequency, and 50% duty cycle square-wave-voltage as an example.

Keywords: inductor loss estimation, high current detection, B–H analyzer, high-power density, shunt resistor

1. Introduction

Owing to the advances in technology, more and more power electronics applications are developed to meet the needs of human life. How to enhance the power density of converters become an important issue in power converter design. With the significant advancement of the semiconductor devices, e.g. the SiC and GaN materials, the switching frequency of power converters have enable to be increased. The volume of inductor can be effectively reduced because of the improvement of the operating frequency. More attention is paid to the estimation of inductor loss. Several iron loss calculation methods are proposed to realizing the high-power-density converter [(1)–(9)]. In addition, the accurate power losses experimental measurement of inductive components can aid researchers and designers in inductor investigation and loss calculation verification.

At present, the inductor is operated at over 100 A current condition in more and more high-power applications. The B–H analyzer has high accuracy to measure the inductor characteristics. However, it has only maximum ±30 A DC bias current and ±6 A AC ripple current testing conditions. It cannot deal with the high current measurement condition.

One of the proposed method was the calorimetric determination method [(7)], which has high accuracy and immune against EMI phase errors features. However, the copper and iron losses of inductor cannot be distinguished, and a high cost temperature chamber is required. In other measurement method, the inductor loss measurement was established as measuring the voltage of primary or secondary winding and the current of primary winding of inductive components [(8)], as shown in Fig. 1. Accordingly, the copper and iron losses measurement can be analyzed, respectively. In this configuration, a shunt resistor, such as non-inductive resistor, with very small associated stray inductance and capacitance is required as a current detector. However, the parasitic inductance could not be zero even if it cancelled out the magnetic fields by manufacturing the inside of resistor structure. The small parasitic inductance could make the current error detection as a result of inductor loss calculated deviation. In addition, the parasitic inductance might be increased when high power rating resistor is used or numbers of resistors are paralleled for measuring higher power/current inductor, such as 100 A, 200 A, 300 A.

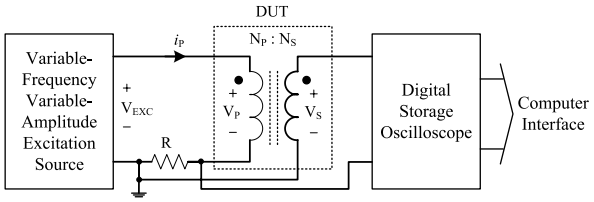

Fig. 1. Inductor loss measurement setup with digital oscilloscope [(8)]

To detect the high inductor current conditions, another detecting method is using Hall Effect current probe. At present, the rated current of AC/DC current sensor is up to 500 A. However, the frequency characteristics of current sensor are extremely influence the measurement accuracy because of the phase shift errors on each harmonic components [(8)(9)]. To solve this problem, the phase error correction method for current probe was proposed [(9)]. By adjusting the phase error of each harmonic components, the measurement accuracy can be greatly improved. However, the measurement results is very sensitive to the corrected phase errors of current probe, as a result, the high precisely measurement instrument, B–H analyzer, is required to measure the frequency characteristics

a) Correspondence to: Pin Yu Huang. E-mail: pyhuang@kit.ac.jp
* Kyoto Institute of Technology
Matsugasaki, Sakyo-ku, Kyoto 606-8585, Japan
** Tokyo Metropolitan University
1-1, Minami-osawa, Hachioji, Tokyo 192-0397, Japan

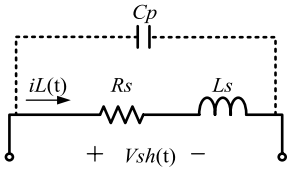

Fig. 2. Equivalent circuit of shunt resistor

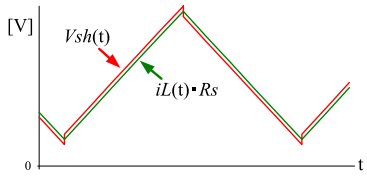

Fig. 3. Voltage waveforms of shunt resistor

of used current probe.

In summary, shunt resistor is considered as the low-cost current-sensing candidates. However, the significant drawback has to overcome that the parasitic components lead to the current detecting deviation especially for numerous paralleled resistors under high power measurement conditions. The current unbalance distribution of each shunt resistors further increasing the difficult of inductor current detection. In this paper, a parallel-connected configuration of shunt resistor is proposed for measuring inductor loss under high current amplitude condition. Moreover, the Runge-Kutta calculation of differential equation solution is applied to figure out the inductor current that the result excluded parasitic inductance influence from the sensing voltage of shunt resistor.

2. Runge-Kutta Method for Inductor Current Calculation

Figure 2 is the generally used equivalent model of shunt resistor which include the series-connected parasitic inductor and parallel-connected parasitic capacitance. To simplify the analysis, the parasitic capacitance is not considered in this paper. The influence of parasitic capacitance is small enough to be ignored.

While using shunt resistor as the current detection of inductor loss measurement, the parasitic inductance result in the measurement deviation. For instance, the triangular inductor current through the parasitic inductance makes additional square waveform on entire voltage of shunt resistor, as shown in Fig. 3.

The practical current of inductor through shunt resistor could be found as a first order differential equation as expressed in (1).

$$\frac{d}{dt}iL(t) = \frac{Vsh(t)}{Ls} - \frac{iL(t)\cdot Rs}{Ls} \cdots\cdots\cdots\cdots\cdots\cdots (1)$$

The Runge-Kutta method is a good candidate for numerical solutions of differential equations. In this paper, the current of inductor is calculated by using the classic Runge-Kutta method, RK4. The explicit Runge-Kutta mathematically calculation is represented in the appendix of paper. Several software, e.g. Matlab, could help in executing the calculation.

3. Proposed Shunt Resistor

3.1 Configuration The parallel-connected configuration is generally used when the power rating of inductor

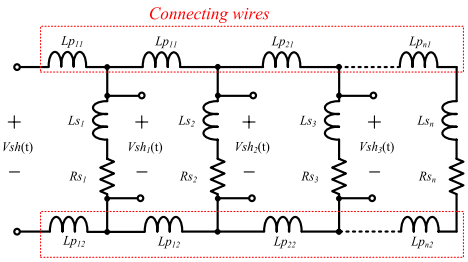

Fig. 4. Equivalent circuit of parallel-connected shunt resistor

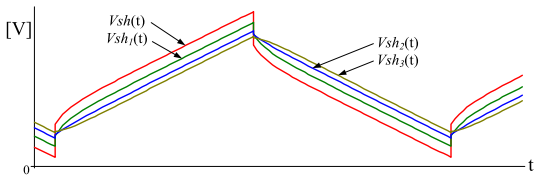

Fig. 5. Voltage waveforms of each shunt resistor in parallel-connected configuration

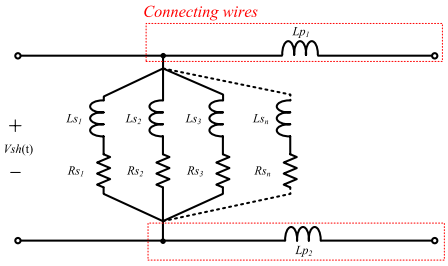

Fig. 6. Equivalent circuit of proposed shunt resistor connecting method

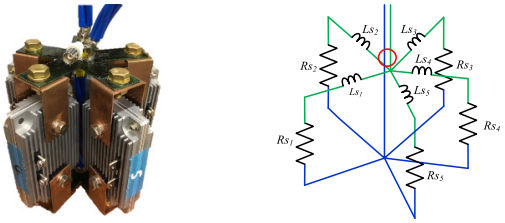

(a) Practical view (b) Equivalent circuit

Fig. 7. Proposed shunt resistor bank

measurement is further increased, as shown in Fig. 4. However, the connecting wires make additional parasitic inductor and increased as follow the number of parallel unit. In Fig. 5, each of current loops contains different parasitic inductances that the unbalanced current wave shape resulted in the calculation and measurement difficulties increased.

In order to alleviate the detecting errors cause by the unbalance current issue, the symmetrical construction is used. The equivalent circuit of proposed connecting concept is illustrated in Fig. 6. The symmetrical construction allow the parasitic inductance on each paralleled component to be as close as possible.

Figure 7 is the practical view and equivalent circuit of the proposed parallel-connected shunt resistor bank. It consists of five shunt resistor units. The issue of parasitic inductance unbalanced can be solved by means of symmetrical construction. In addition, more shunt resistor units are possible to combine in parallel when measurement power rating is increased.

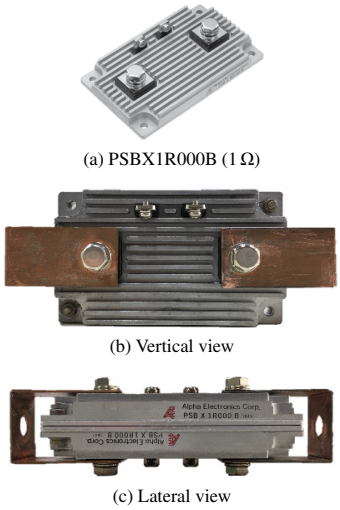

(a) PSBX1R000B (1 Ω)

(b) Vertical view

(c) Lateral view

Fig. 8. One unit of proposed shunt resistor

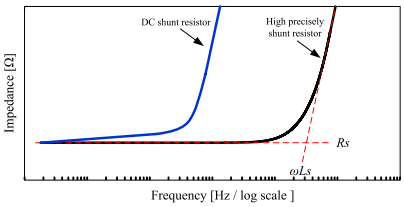

Fig. 9. Frequency characteristics of recommended shunt resistor

In high power rating inductor loss measurement, the large volume of shunt resistor bring about difficult task of measurement points setup. For example, the wide distance of two measurement terminals resulted in long grounding wires of probe and easily coupling the magnetic flux which cause by the high measurement current. To alleviate this problem, two measurement terminals are set as close as possible in proposed shunt resistor. As shown in Fig. 7(b), the red circle indicated the current signal measurement point of the proposed configuration. Therefore, the BNC adaptor can be used to connect the tip of oscilloscope probe directly. The measurement accuracy can be improved by minimizing the grounding wire of probe.

Each shunt resistor unit consists of two parallel-connected ultra-precision shunt resistors, PSBX1R000B, which has very good frequency and temperature characteristics. Figure 8 shows the single component, the vertical, and the lateral views of one shunt resistor unit, respectively. The resistors are connected with the biggest contact area of their heat sink. This configuration can help the resistors have well heat distribution in high power rating inductor loss measurement.

3.2 Frequency Characteristic In order to improve the accuracy of Runge-Kutta method calculation, the resistance and parasitic inductance of shunt resistor, Rs and Ls, have to be considered as constant real number in (1). Therefore, a shunt resistor which has better frequency and temperature characteristics compared with the general-used DC shunt resistor is preferred to used, as shown in Fig. 9.

Two steps are used to realize the equivalent components of proposed shunt resistor bank. First, it has to measure the frequency dependence of impedance. Second, selecting the sufficient high and low frequency points to calculate the

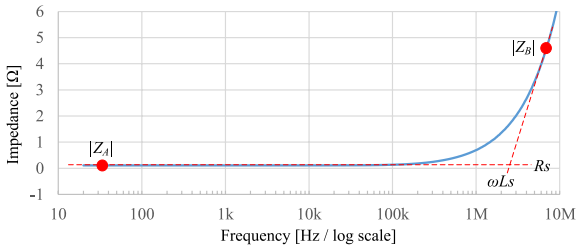

Fig. 10. Equivalent components evaluation of shunt resistor method

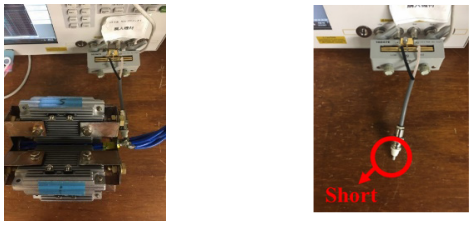

(a) Total testing shunt resistor (b) Connected cable wire

Fig. 11. Frequency characteristic measurement setup of proposed shunt resistor bank

equivalent components as shown in Fig. 10. The resistance and parasitic inductance are expressed as (2) and (3), respectively.

$$Ls = \sqrt{\frac{|Z_B|^2 - |Z_A|^2}{\omega_B^2 - \omega_A^2}} \quad \cdots\cdots (2)$$

$$Rs = \sqrt{|Z_A|^2 - (\omega Ls)^2} \quad \cdots\cdots (3)$$

The accurate value of equivalent components are significant parameters in Runge-Kutta calculation. Thus, removing the possible measurement errors is necessary. In particular, long testing wires used to measure the large volume of shunt resistor which cause the deviation in equivalent components measurement. In proposed configuration, the both ends of shunt resistors are set to one measurement point resulted in reducing the error of frequency characteristic measurement. In addition, the short and low-noise cable wire is preferred to minimum the deviation. As shown in Figs. 11(a) and (b), the impedance and phase angle are respectively measured with total testing shunt resistor and connected cable wire. The correctly equivalent components of proposed shunt resistor can be realized by subtracting parasitic components of the connected cable wire. The measurement results and calculation verification of impedance and phase angle are illustrated in Figs. 12(a), (b), (c) and, (d), respectively. The specification of proposed shunt resistor is represented in Table 1.

4. Measurement Setup

Figure 13 shows the inductor measurement system which used in this study. It is an energy circulating measurement system. The device under test (DUT) of measured inductor is set to the output inductor of buck converter. Thus, the inductor is operated and measured under square-wave-voltage condition. In addition, the voltage and current of measured inductor can be controlled to target value through system feedback control. The output capacitor of buck converter, C_2, is considered as an input capacitor of the boost converter and then transfer the energy back to the input capacitor of buck

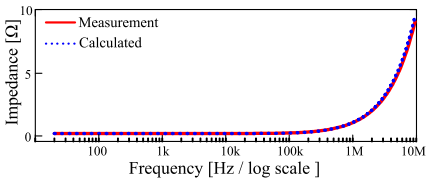

(a) Impedance of total testing shunt resistor

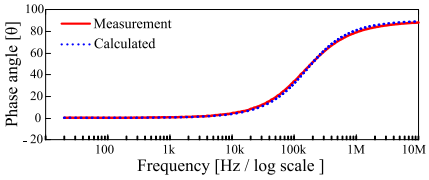

(b) Phase angle of total testing shunt resistor

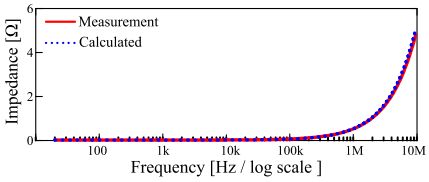

(c) Impedance of connected cable wire

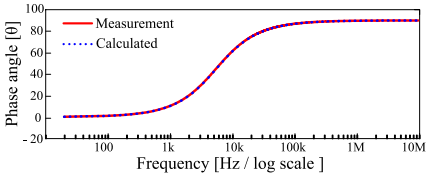

(d) Phase angle of connected cable wire

Fig. 12. Frequency characteristic measurement and calculation results verification of proposed shunt resistors

Table 1. Specification of Proposed Shunt Resistors Bank

Parameters	Value
Used Ultra-precision Resistor	PSBX1R000B (1 Ω)
Number of Paralleled Resistors	10
Total Resistance, *Rs*	0.1009 Ω
Parasitic inductance, *Ls*	67.59 nH

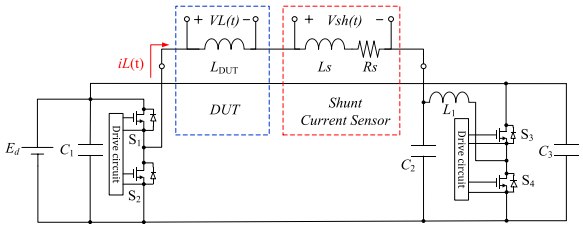

Fig. 13. Inductor power loss measurement system

converter, C_1. Therefore, the power supply only need to provide the energy for inductor power loss and system energy dissipation. The proposed shunt resistors bank is series connected to the DUT for inductor current detection.

In this paper, the sampling rate of oscilloscope is set to 100 M/s because one period with 10000 points of voltage and current data are required for Runge-Kutta Method, where the switching frequency is 10 kHz. In addition, the time scale of oscilloscope is set to 200 μs/div for 20 periods, namely 200000 data for one waveform.

A low attenuation probe is recommend to maximize the oscilloscope's vertical sensitivity. In addition, the sufficient bandwidth and high input impedance of measurement instrument is preferred. Therefore, the 10X passive probes with IWATSU isolation amplifier (SE - 6000/SE - 6010) are applied to the measurement system. In addition, the proposed shunt resistors bank is put in the water cooling tank to enhance the measurement power rating. Meanwhile, the shunt resistor can operate under well temperature distribution condition.

5. Measurement Calibration

Although some of tips are very basic for power electronics engineers, this section introduce the inductor loss measurement calibration procedures in detail. For obtaining accurate results, the measuring steps have to consider the measurement error carefully. First, the instruments include oscilloscope, probes, amplifier for probes, energy circulating measurement system, etc. are required enough warming up time before testing inductor loss. Next, calibrating the following errors when measuring different inductor operating conditions.

5.1 Calibrate the Deskew Function Value The phase displacement between the probes should be corrected [8]. The relative error in percentage, k, can be expressed as (4), where θ denotes the actual phase angle between voltage and current and $\Delta\varphi$ the phase error between the voltage and current sensor.

$$k = \frac{\cos(\theta + \Delta\varphi(f)) - \cos(\theta)}{\cos(\theta)} \times 100\,[\%] \cdots\cdots\cdots (4)$$

Using rectangular waveform as an input signal could calibrate the phase error easily.

5.2 Calibrate the DC Offset Error of Probes The DC offset errors are inherent in the oscilloscopes and probes. The inductor loss measurement deviation of DC offset error can be calculated in (5) to (8), where the phase displacement is not considered; $iL(t)_{osc}$ and $VL(t)_{osc}$ are the measured current and voltage waveforms of inductor from oscilloscope; $iL(t)_{real}$ and $VL(t)_{real}$ are real current and voltage of inductor; iL_{dc_offset} and VL_{dc_offset} assume the offset error value; $iL_{average}$ is the average value of inductor.

$$iL(t)_{osc} = iL(t)_{real} + iL_{dc\_offset} \cdots\cdots\cdots (5)$$

$$VL(t)_{osc} = VL(t)_{real} + VL_{dc\_offset} \cdots\cdots\cdots (6)$$

$$P_{loss} = \frac{1}{T}\int [VL(t)_{osc} \cdot iL(t)_{osc}]dt \cdots\cdots\cdots (7)$$

$$P_{loss\_error} = VL_{dc\_offset} \cdot (iL_{average} + iL_{dc\_offset}) \cdots\cdots (8)$$

Figure 14 shows calculation results of the inductor power loss deviation when the probes have different DC offset errors. The calculation results of inductor power loss error are made under 100 A (RMS) current, ±100 V voltage, 10 kHz switching frequency, and 50% duty cycle square-wave-voltage conditions. The DC offset errors are represented in a percentage of average current and peak voltage of inductor, respectively. As shown in Fig. 14, the DC offset error of voltage probe greatly affect to the inductor power loss measurement. Only 0.5 V (0.5%) DC offset error of inductor voltage leads the inductor loss measurement to 50 W deviation. To abbreviate these problems, the DC offset and phase calibrations are strongly recommended before beginning the inductor power loss measurement. Furthermore, the

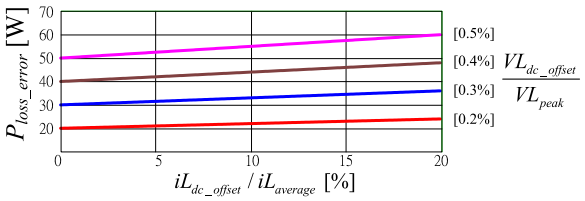

Fig. 14. Inductor power loss deviation corresponding to different DC offset errors of probes under 50% duty cycle, ±100 V square-wave-voltage, 10 kHz switching frequency, and 100 A (RMS) current conditions

Table 2. Inductor Measurement Conditions

Parameters	Value
Inductance	209 μH
Switching frequency	10 kHz
Voltage of inductor	± 100 V
Duty cycle	50 %
Inductor current	10 A (RMS) ~ 160 A (RMS)

value of DC offset errors will be changed with the different attenuations and the scales of channel.

However, the amplitude of DC offset errors is floating depending on the sampling rate and channel scales of digital oscilloscope. In proposed method, 200,000 point data per waveform are used for Runge-Kutta calculation. Higher sampling rate could improve the measurement accuracy but lead extremely large data processing. In this paper, the calibration procedures for finding the floating DC offset error value are firstly short-circuit the voltage probes and using average function of oscilloscope to get one reference data of each probe. Then, repeat over ten times to get an averaging DC offset error.

6. Experimental Results

6.1 Proposed Inductor Loss Measurement To demonstrate the measurement method feasibility, the total loss of inductor is measured with proposed method as an example. The measurement conditions are listed in Table 2.

As shown in Fig. 15, the measurement resuls are compared with high accuracy current probe, HIOKI CT6904, and high precisely power analyzer, PPA5530. The maximum measured current range of common used power analyzer, PPA5530, is limited to 30 Ampere. As shown, the results of two different methodologies are basically matched under 30 A current conditions. It could be found that two methods have same accuracy on inductor loss measurment. For more high power application, the high accuracy current probe with the phase correction function has used to compare with proposed method [9]. It seems the similar measurement results that provide the solutions in high power/current inductor measurement. Although the phase correction is inherent in the high-priced CT6904, the further precisely phase corretion might be required for measuring correctly. Accordingly, the proposed method provide a potential solution to measure the inductor loss at high current conditions as a low-cost methodology.

The Runge-Kutta method is applied to calculate the practical inductor current. Without considering the parasitic inductance effect in inductor current-sensing, the significant

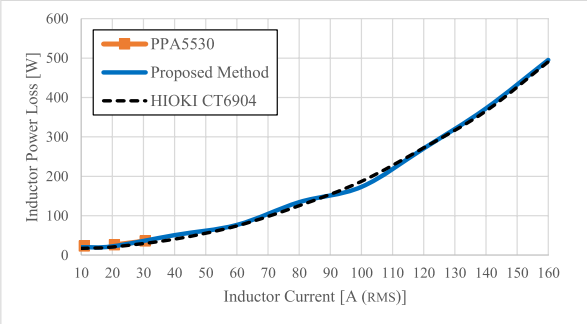

Fig. 15. Total loss comparison of power analyzer, PPA5530, proposed method, and HIOKI CT6904

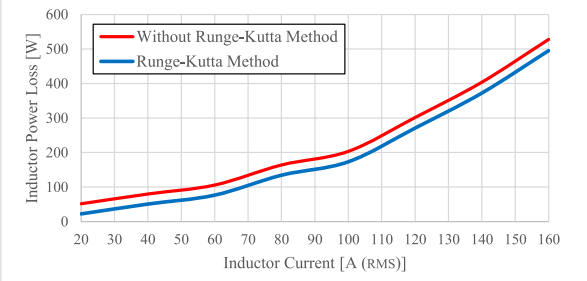

Fig. 16. Measurement results with corresponding Runge-Kutta calculation method

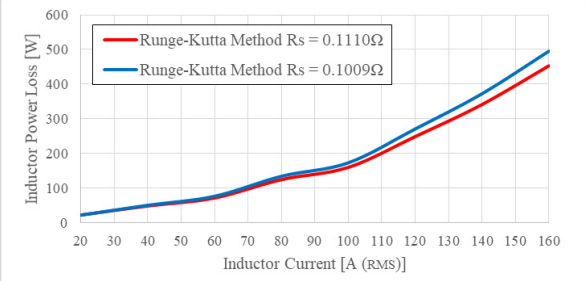

Fig. 17. Runge-Kutta calculation method with resistance deviation, Rs = 0.111 Ω and 0.1009 Ω

measurement error was occurred as shown in Fig. 16.

To demonstrate the influence of accurate equivalent components of used shunt resistor on inductor loss measurement results, the resistance and parasitic inductance are set up to 10% difference as measurement errors in Fig. 17 and Fig. 18, respectively. In Fig. 17, the deviation of inductor loss is increasing follow the current condition and has 50 W difference at 160 A condition. It is intuitional view that the resistance directly influent the detecting current. In Fig. 18, the results of inductor loss basically are identical with different parasitic inductance of shunt resistor. It is considered that parasitic inductance will indirect influence the detecting voltage of shunt resistor. However, the value is quite small that 10% difference doesn't have significant changed in measurement results.

DC offset errors of are floating value depending on different setup of probes and oscilloscope include attenuation, sampling rate, scales, etc. The calibration of each probe has to be done before starting the inductor loss measurement. Figure 19 shows the measurement results with and without DC offset correction. As shown, the deviation increasing significantly under high current measurement conditions. It

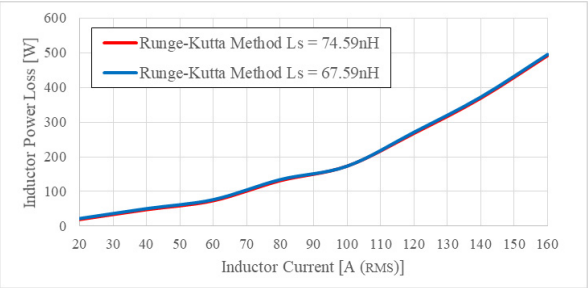

Fig. 18. Runge-Kutta calculation method with parasitic inductance deviation, Ls = 74.59 nH and 67.59 nH

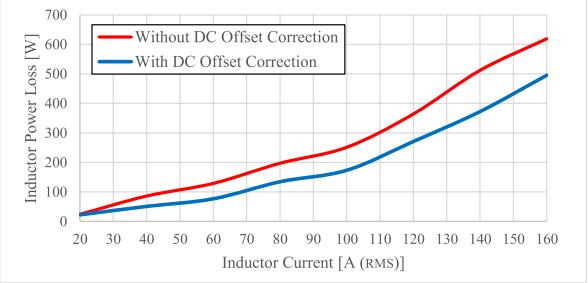

Fig. 19. Measurement results with corresponding DC offset correction

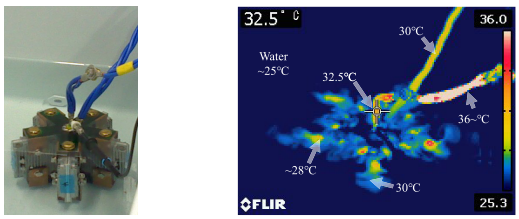

Fig. 20. Temperature distribution of proposed shunt resistor under 160 A (RMS) inductor current condition

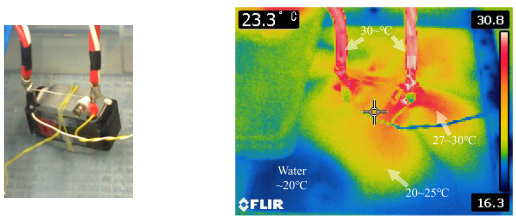

Fig. 21. Temperature distribution of DUT under 160 A (RMS) inductor current condition

could be found in (8) that the power loss error increases follow the average current of inductor. Additionally, the measuring scale of channel switched to bigger range resulted in decreasing the accuracy of measuring waveform and different DC offset error.

Figure 20 and Fig. 21 respectively shows the temperature distribution of proposed shunt resistors bank and DUT under 160 A (RMS) inductor current and continuous 30 seconds operating conditions. The temperature is uniform distributed by means of the water cooling tank and designed configuration.

The temperature coefficient influence the results of inductor loss measurement indeed. However, the high current condition increase the difficulty and cost of measurement system design for reaching the steady state temperature of DUT and shunt resistor. In the proposed method, the measurement system which used in Fig. 13 was designed in around 1 second on-state operation and 1 to 2 seconds off-state operation to minimum the temperature influence. In addition, Fig. 20 and Fig. 21 show the temperature distribution when system continue operated over 30 seconds. It could be considered that the cooling container repressed the temperature rise of DUT and shunt resistor in short time period (1s) of measurement setup condition.

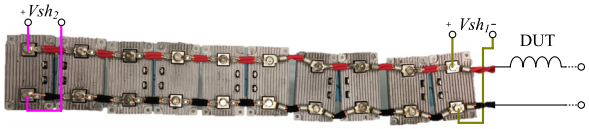

Fig. 22. Horizontal parallel-connected configuration as presented in Fig. 4

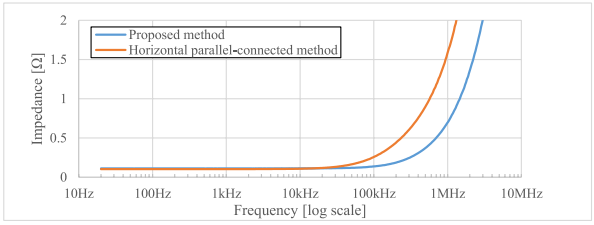

(a) Impedance of proposed method and horizontal parallel-connected method

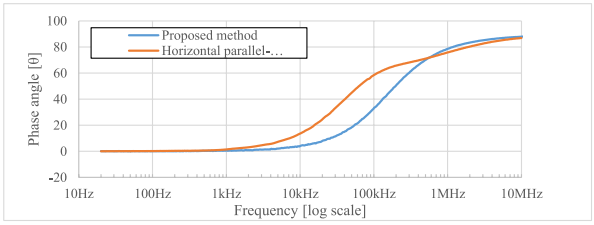

(b) Phase angle of proposed method and horizontal parallel-connected method

Fig. 23. Frequency characteristic comparison between proposed method and horizontal parallel-connected method

6.2 Measurement Comparison with Other Structure of the Shunt Resistor For high power/current measurement, the general solution is used the parallel configuration. However, the voltage and current detection are extremely sensitive to inductor loss measurement. Therefore, there are two important issues for shunt resistor design which including the correctly total voltage detection and better frequency characteristic for obtaining equivalent components in Runge-Kutta calculating method.

To demonstrate the feasibility, two different configurations of shunt resistor bank with same resistance are made and measured the inductor loss, respectively. Figure 22 shows the horizontal parallel-connected shunt resistors. The long-connected structure makes the parasitic components increase and unbalance on each resistors.

As shown in Fig. 23, it could be found that the total inductance of horizontal parallel-connected method is much bigger than the propposed method. Furthermore, the long-connected structure makes the complex frequency characteristic resulted in the difficulty of equivalent components calculation for Runge-Kutta method. Figure 24 represented the measurement results with two different configurations of shunt resistor bank. As shown, the horizontal parallel-connected structure has large deviation on inductor loss mea-

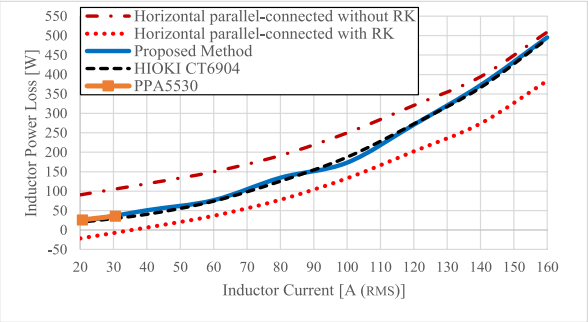

Fig. 24. Total loss comparison between proposed method and horizontal parallel-connected method

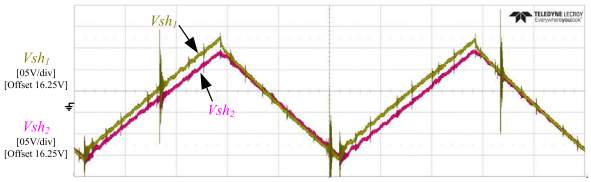

Fig. 25. Voltage imbalance issue on horizontal parallel-connected method

surement. In addition, the voltage imbalance issue of horizontal parallel-connected shunt resistor bank can be found in Fig. 25.

7. Conclusion

A high power rating inductor loss measurement method is achieved by means of shunt resistor current detection. The proposed connection configuration of shunt resistors make identical parasitic inductance on each of paralleled current loops. In addition, by using the Runge-Kutta calculation method, the inductor current can be figured out to minimum the parasitic inductor effects of current detection. The inductor is measured under 10~160 A (RMS) current, 10 kHz switching frequency, and 50% duty cycle square-wave-voltage measurement conditions. The measurement results with proposed method are compared with power analyzer, PPA5530, under 10~30 A (RMS) current conditions. For 30~160 A (RMS) current conditions comparison, a high bandwidth and phase corrected current probe, HIOKI CT6904, is used to verify the feasibility of proposed method. In addition, two different configurations of shunt resistor bank with same resistance are made to compare the inductor loss measurement.

The inductor loss measurement is extremely sensitive to measurement instruments and detecting components, such as temperature, DC offset errors, phase errors, parasitic components, and so on. Power analyzer and B–H analyzer provide high precisely loss measurement for inductor loss but limit in low current conditions. In this paper, a 16 kVA inductor loss measurement is demonstrated as an example. However, there are lots of high power applications at present. The inductor could be operated at 80 kVA (400 V/200 A) or further. Thus, a potential high current inductor loss measurement method with a low-cost shunt resistor current detection is presented.

Acknowledgment

The authors gratefully acknowledge the contribution of Yoshio Bizen and Hiroaki Matsumori for their technical support. This work was supported by Council for Science, Technology and Innovation (CSTI), Cross-ministerial Strategic Innovation Promotion Program (SIP), “Next-generation power electronics”. (Funding agency: NEDO)

References

(1) M. Sippola and R.E. Sepponen: “Accurate prediction of high-frequency power-transformer losses and temperature rise”, IEEE Transactions on Power Electronics, Vol.17, No.5, pp.835–847 (2002)
(2) K. Venkatachalam, C.R. Sullivan, T. Abdallah, and H. Tacca: “Accurate prediction of ferrite core loss with nonsinusoidal waveforms using only Steinmetz parameters”, 2002 IEEE Workshop on Computers in Power Electronics, pp.36–41, Mayaguez, Puerto Rico, USA (2002)
(3) S. Iyasu, T. Shimizu, and K. Ishii: “A novel iron loss calculation method on power converters based on dynamic minor loop”, 2005 European Conference on Power Electronics and Applications, pp.9–10 (2005)
(4) T. Shimizu and S. Iyasu: “A practical iron loss calculation for AC filter inductors used in PWM inverters”, IEEE Transactions on Industrial Electronics, Vol.56, No.7, pp.2600–2609 (2009)
(5) J. Muhlethaler, J. Biela, J.W. Kolar, and A. Ecklebe: “Improved core-loss calculation for magnetic components employed in power electronic systems”, IEEE Transactions on Power Electronics, Vol.27, No.2, pp.964–973 (2012)
(6) N. Kurita, K. Onda, K. Nakanoue, and K. Inagaki: “Loss estimation method for three-phase AC reactors of two types of structures using amorphous wound cores in 400-kVA UPS”, IEEE Transactions on Power Electronics, Vol.29, No.7, pp.3657–3668 (2014)
(7) D. Christen, U. Badstuebner, J. Biela, and J.W. Kolar: “Calorimetric power loss measurement for highly efficient converters”, The 2010 International Power Electronics Conference, pp.1438–1445 (2010)
(8) V.J. Thottuvelil, T.G. Wilson, and H.A. Owen: “High-frequency measurement techniques for magnetic cores”, IEEE Transactions on Power Electronics, Vol.5, No.1, pp.41–53 (1990)
(9) H. Matsumori, T. Shimizu, K. Takano, and H. Ishii: “Evaluation of iron loss of AC filter inductor used in three-phase PWM inverters based on an iron loss analyzer”, IEEE Transactions on Power Electronics, Vol.31, No.4, pp.3080–3095 (2016)

Appendix

The Runge-Kutta method is one of implicit and explicit iterative methods. It is used to solve the differential equations in (1). In this paper, the “RK4” is used and the relative equations expressed from (A1) to (A6).

$$y_{n+1} = y_n + \frac{1}{6}(k_1 + 2k_2 + 2k_3 + k_4) \quad \cdots\cdots\cdots\cdots (A1)$$

$$t_{n+1} = t_n + h \quad \cdots\cdots\cdots\cdots (A2)$$

$$k_1 = h \cdot f(t_n, y_n) \quad \cdots\cdots\cdots\cdots (A3)$$

$$k_2 = h \cdot f\left(t_n + \frac{h}{2}, y_n + \frac{k_1}{2}\right) \quad \cdots\cdots\cdots\cdots (A4)$$

$$k_3 = h \cdot f\left(t_n + \frac{h}{2}, y_n + \frac{k_2}{2}\right) \quad \cdots\cdots\cdots\cdots (A5)$$

$$k_4 = h \cdot f(t_n + h, y_n + k_3) \quad \cdots\cdots\cdots\cdots (A6)$$

Here, y_n is replaced to solution of differential equation which represent inductor current, iL_n. The h is equal to 10 ns which represent the step-size, 10000 data in one period. The f function represent the differential value of inductor current, diL/dt. Consequently, the inductor current approximation could be obtained by (A1) to (A6). The mathematical software or MATLAB could help in executing the calculation easily.

Pin-Yu Huang (Member) was born in Taipei, Taiwan, in 1985. He received the M.S. and Ph.D. degrees in electrical engineering from National Taiwan University of Science and Technology, Taipei, Taiwan, in 2011, and 2015, respectively. In 2013, he was a Visiting Scholar at The Center for Power Electronics (CPES), Virginia Polytechnic Institute and State University, USA. From 2015 to 2018, he was a Postdoctoral Researcher in the Tokyo Metropolitan University Power Electronic Laboratory, Japan. He is currently an assistant professor in Kyoto Institute of Technology since 2018. His current research interests include voltage multiplier, high power density dc-dc converter design, multi-level converter, passive components characteristics measurement of capacitors and inductors, 3 port power router for renewable energy dc microgrid, etc.

Toshihisa Shimizu (Fellow) was born in Tokyo, Japan, in 1955. He received the B.E., M.E., and Dr.Eng. degrees in electrical engineering from Tokyo Metropolitan University, Tokyo, Japan, in 1978, 1980, and 1991, respectively. In 1998, he was a Visiting Professor at Virginia Power Electronics Center (VPEC), Virginia Polytechnic Institute and State University, USA. He joined Fuji Electric Corporate Research and Development Ltd. in 1980. Since 1993, he has been with Department of Electrical Engineering, Tokyo Metropolitan University, Tokyo, Japan, where he currently a Full Professor. His current research interests include power converters, high-frequency inverters, photovoltaic power generations, UPSs, EMI problems, high power density converter design, inductor loss analysis, etc. He is an Associate Editor of the Transactions on Power Electronics. He has authored or coauthored more than 100 journal papers and 120 international conference proceedings and 6 technical books. He also holds ten patents and more than ten patents pending. Dr. Shimizu has received transactions paper awards from the Institute of Electrical Engineers of Japan in 1999 and 2010. Five best paper awards at International Power Electronics Conference (IPEC2010-ECCE Asia), European Power Electronics-Power Electronics and Motion Control Conference (EPE-PEMC2010), and ECCE2015-7, respectively. He is a Fellow Member of the Institute of Electrical and Electronics Engineers (IEEE) and Institute of Electrical Engineers of Japan (IEEJ).